Pergamon

Cement and Concrete Research, Vol. 26, No. 2, pp. 295-307, 1996

0008-8846/96 $15.00 + .00

SSDI 0008-8846(95)00202-2

HEAT CURING AND POST-HEAT CURING REGIMES OF HIGH- PERFORMANCE CONCRETE: INFLUENCE ON MICROSTRUCTURE AND C-S-H COMPOSITION

Knut O. Kjellsen
Swedish Cement and Concrete Research Institute
100 44 Stockholm, Sweden

(Refereed)
(Received July 28, 1995; in final form October 10, 1995)

ABSTRACT

The present work reports a study on the effect of heat curing and post-heat curing conditions on the microstructure and C-S-H composition of a high-performance concrete. In addition, some previously studied cement paste specimens of ordinary w/c ratio hydrated at various temperatures have been reanalyzed. Heat cured high-performance concrete showed a higher hollow shell porosity at later ages than a normally cured companion. Apparently the distribution of C-S-H throughout the cement paste matrix of the high-performance concretes was not significantly influenced by heat curing. However, the composition of the C-S-H phases was influenced by the curing regimes. The effect of heat curing on the microstructure appears to differ between high-performance and ordinary concretes.

Introduction

Concrete outside the laboratory cures at temperatures other than 20°C and often under less than ideal moisture conditions. High curing temperatures may result from hot weather, accumulated heat of hydration or applied heat. Heat curing is used in the production of precast concrete products primarily in order to increase the early-age strength to allow for rapid production. It is often observed, however, that long-term properties are negatively influenced by elevated curing temperatures. Strength and other mechanical properties are often reduced and permeability increased (1-3). It has been shown that curing at elevated temperatures may influence the microstructure considerably. Based on determination of the BET region of sorption isotherms and mercury intrusion porosimetry experiments (MIP), it has been reported that curing at elevated temperatures leads to reduced surface areas of the hydrates formed and a coarser pore structure (4-7). From scanning electron microscopy (SEM) studies it has been reported (8,9) that a coarser pore structure of the "outer" (10) or "undesignated" (11) product phase prevailed at mature ages as a result of isothermal curing at elevated temperatures. It was reported that the distribution of reaction products was much more uniform in pastes cured at relatively low temperatures. In pastes cured at high temperatures, relatively dense shells of reaction products formed around the hydrating cement grains, while the outer product phase

remained relatively porous as relatively little reaction product formed in this phase. These observations were in agreement with the hypothesis of Verbeck and Helmuth (12). Other effects of curing at elevated temperatures may occur under certain conditions. Curing at temperatures above about 70°C at early ages may influence the formation of ettringite decisively as this phase may not form at higher temperatures (13-16). At even higher temperatures monosulfate also becomes unstable and hydrogarnet may occur. Ettringite can reform at later ages, resulting in destructive cracking. Another effect of heat curing is that caused by a too rapid temperature rise at early ages, which may lead to microcracking and increased porosity due to differences in the thermal properties of the concrete constituents (17).

The motive of the present work was to provide information about the microstructure and chemical composition of the C-S-H phases of heat cured high-performance concrete. Such information can be helpful in understanding the mechanisms of heat curing in high-performance concrete. The mechanical and physical properties of the same concretes have also been studied and will be reported elsewhere[1]. Curing cycles similar to those used in the production of precast products were simulated in the laboratory. The effects of heat treatment and post-heat curing conditions were studied. The post heat-curing conditions involved quite severe drying. For comparison, some previously studied cement paste specimens hydrated at various temperatures (8,9) are reanalyzed.

Experimental

Materials, Mixing and Casting. One high-performance concrete and one cement paste having a water/cement (w/c) ratio of 0.5 were studied in the present work. The pure cement paste specimens have been studied previously (8,9) where details of the experimental procedures are reported. The cement used in (8,9) corresponded to ASTM Type I/III. The high-performance concrete had a water/binder (w/b) ratio of 0.31, the binder comprised 95% cement and 5% silica fume by mass. The concrete contained 505 kg/m^3 binder, 858 kg/m^3 sand and 929 kg/m^3 coarse aggregate. The amount of superplasticizer was 1.8%. The superplasticizer (33% solids) was of the melamin type and the silica fume was in slurry form (50/50). The cement used was a Swedish sulfate resistant cement (ASTM Type V) with chemical composition (weight percent); 22.2% SiO_2, 3.4% Al_2O_3, 4.8% Fe_2O_3, 64.9% CaO, 0.91% MgO, 0.56% K_2O, 0.04% Na_2O, 2.0% SO_3, 0.63% ignition loss. The Blaine specific surface and density were 302 m^2/kg and 3220 kg/m^3, respectively. The Bogue composition were; 19.8% C_2S, 58.1% C_3S, 0.8% C_3A, 14.5% C_4AF. The silica fume contained 94.2% SiO_2, had a loss on ignition of 1.8% and a specific surface of 23.0 m^2/gram. The aggregates were taken from a local glacifluvial granitoid deposit (Underås). The sand fraction (0-8 mm) had a fineness modulus of 3.09 according to Swedish Standard 132126. The coarse aggregate fraction (8-16 mm) was partly crushed. The coarse fraction was washed in order to reduce the amount of fines and increase the homogeneity of the aggregate.

The mixer used was of the pan type and batches of 110 liters were produced. The cement and aggregates were first blended for 2 minutes. The water was then added and mixed for 30 seconds before the silica slurry was added. After a short mixing period the superplasticizer was added and the mixing continued for 3 more minutes. The concretes were cast in forms which

[1] Kjellsen, K.O., presented at 1995 MRS Fall Meeting.

were sealed in plastic bags. Mixing and curing through the preset period (Fig.1) took place at 20°C.

Curing Procedures. The aim of the experiments was to study the effect of heat curing and subsequent drying on the microstructure and properties of high-performance concrete. Heat curing regimes and post-heat curing conditions which may occur in the precast concrete industry were simulated. The heat curing regimes is shown in Fig.1. Curing cycle A, constant 20°C curing in limewater, served as a reference curing regime. Curing cycle B was as shown in Fig.1 with subsequent limewater curing at 20°C. Curing cycle C was the heat curing regime as B, but with subsequent outdoor storage. Precast products are normally cured similarly to cycle C. After heat curing and demolding, precast products are often brought to an outdoor storage site where they are exposed to the prevailing weather conditions. After the preset period the sealed specimens were transferred to curing tanks and submerged in circulating water which was gradually heated. The temperature was measured by thermocouples in dummy specimens; Fig.1 depicts the actual concrete temperatures. About 6 hours after the cooling period, the specimens were demolded and the cycle A and B specimens placed in 20°C water while the specimens of cycle C were placed on an unsheltered outdoor storage site for 27 days. The experiments were performed in spring under sunny weather conditions with practically no rainfall. The temperature ranged from 26°C to 3°C, with an average of 13.5°C. Relative humidity ranged from 75% to 38%, with an average of 60%. The average wind speed over the storage period was 2.5 m/s.

Test Methods and Specimen Preparation. Scanning electron microscopy (SEM) and energy dispersive X-ray analysis (SEM-EDX) were the experimental techniques applied. Backscattered electron images of polished sections were obtained and quantitative X-ray analysis performed. The Jeol model 6400 microscope was operated at 10 kV. Backscattered electron images of flat specimens reflect the backscattering coefficient of scattered regions. The backscattering coefficient is basically dependent on the atomic number of the elements present and their mass concentration. The higher the atomic number of the elements present in a phase and/or the higher their concentration the brigther the phase appear in the image. In hydrated cement paste or concrete the unhydrated cement grains should appear nearly white, calcium hydroxide light gray, other hydration products generally darker gray, and pores black or nearly so. In back-

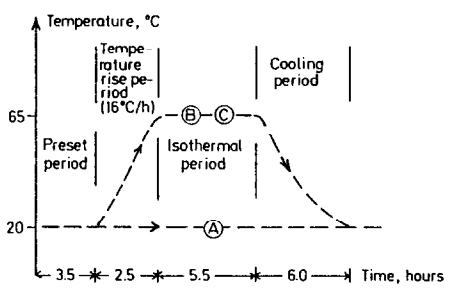

FIG.1
Curing regimes.

scattered electron images phases of C-S-H with, for example, the same Ca/Si ratio as C_2S will appear darker than C_2S as a result of the presence of water and pores in the C-S-H phase. The gray level range of the C-S-H phases will generally be much wider than that of the other phases present because of its more variable composition and structure. SEM-EDX analysis was performed as point analysis. The inner and outer reaction product phases, originally defined by Taplin (10) as those products deposited within and outside the original cement grain boundary, respectively, were analyzed. Microanalyses were performed only in the bulk paste phase of the concretes and only the data pertaining to the C-S-H were accounted for in the presentation of the numerical results. The analysis of inner products was performed in phenograins (18) containing inner products and remnant anhydrous particles consisting mainly of alite, as inner product of C-S-H wide enough for reliable microanalysis seldom form around belite grains after 28 days. Analyses of the outer product phase were made more arbitrarily but always at spots considered to be essentially C-S-H. Of each specimen, at least 15 analyses were performed in each of the inner and outer product phases. Several fields of each specimen were studied. Additional point analyses were performed in order to identify various phases. The beam current was held at 5 nA yielding a count rate of about 1500 cps measured on a cobalt standard. The counting time was 100s. Matrix corrections were made by the ZAF procedure. Pure elemental or mineral standards of the elements to be analyzed were recorded before the first analysis was performed. The cobalt standard was periodically used for control between analysis of any gain change which may occur in the spectrometer and the beam current was frequently measured in a Faraday cup. Corrections were made as necessary. Analyses were made for Na, Mg, Al, Si, S, K, Ca, and Fe. Oxygen was stoichiometrically calculated, to provide the analysis totals.

Specimens of a few millimeters in dimension were cut from the skin (approximately the first 10 mm from the surface) of 10 cm diameter cylinders by a precision diamond saw. Hydration was stopped by freezing in liquid nitrogen. The specimens were subsequently vacuum dried for 2 days and then dried at 105°C overnight. This combined freeze-drying and oven-drying procedure has been shown to be very gentle in that it induces very little microcracking in the structure. The specimens were then vacuum impregnated with a low viscosity epoxy resin and carefully ground and polished. Alcohol was used as lubricant during cutting and grinding while diamond paste was used as the polishing medium. The specimens were finally made conductive by the application of a thin coating of carbon. Characteristics regarding the quality of the specimen preparation, such as relief effects between hard and soft phases, epoxy filling of larger pores and "pull outs" were examined by electronmicroscopy in the secondary electron mode and in the topographical backscattered electron mode. Backscattered electron imaging providing topographical information was obtained by subtraction of the signals from the paired semiconductor element detector on the microscope. The more common compositional imaging is obtained by summation of the signals. The specimens showed little relief effects, good epoxy saturation and few "pull outs".

Results

Figs.2, 3 and 4 show relatively low magnification images of the high-performance concrete cured according to curing regimes A, B and C, respectively. Parts of larger aggregate particles are seen towards the edges of the images. It appears that concrete C contains relatively numerous large pores. A more detailed image of the bulk paste phase of this specimen is shown in Fig.5. It can be observed that the majority of the large pores are hollow shells (Hadley

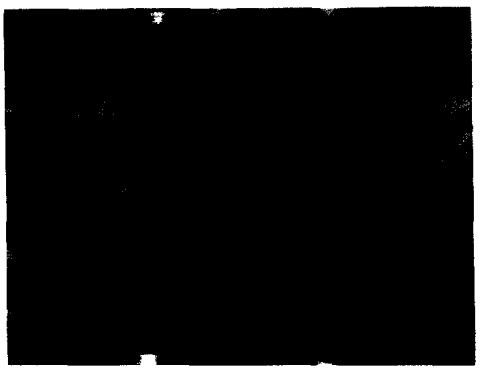

FIG. 2.
Backscattered electron image of the high-performance concrete, subjected to a constant 20°C limewater cure for 27 days.

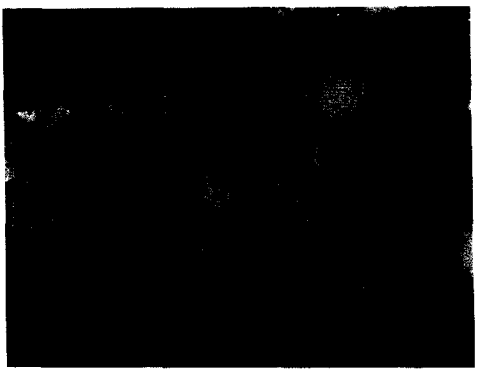

FIG. 3
Backscattered electron image of the high-performance concrete, subjected to simulated steam cure followed by 20°C limewater cure for 27 days.

grains). Large capillary pores and spaces are also apparent. Figs.6 and 7 depict detailed bulk paste phases of concretes A and B, respectively. The large pores in these concretes are also essentially of the hollow shell type. It appears from Figs.2 through 7 that the porosity constituted by hollow shells is larger for concrete C, than for concrete B, which in turn is larger than the hollow shell porosity of concrete A.

FIG. 4.
Backscattered electron image of the high-performance concrete, subjected to simulated steam cure followed by outdoor exposure for 27 days.

FIG. 5.
Detailed image of the concrete shown in Fig.4.

FIG. 6
Detailed image of the concrete shown in Fig.2.

FIG. 7.
Detailed image of the concrete shown in Fig.3.

Curing under less than moisture-saturated conditions is reported to result in higher hollow shell porosities than curing under saturated conditions (19). Under saturated conditions hydrates of C-S-H, CH and AFm deposit increasingly in previously formed hollow shells resulting in reduced hollow shell porosity. Removal of water by drying will at least partially empty the pores, and larger pores will be emptied before smaller pores. Consequently, the mobility of ions and other small species in the microstructure will be reduced. Thus less product forms in the previously formed hollow shells. Although the degree of hydration has not been measured in the present work, it would be expected that concrete C has a lower degree of hydration than the

TABLE 1

Atomic Ratios and Total Oxide of the Inner- and Outer- Product Phases of the 0.31 w/b Ratio Concrete Specimens Cured According to Cycles A, B and C
(Mean values; standard deviations in parantheses)

	HP A		HP B		HP C	
	Inner product	Outer product	Inner product	Outer product	Inner product	Outer product
Total oxide (%)	78.9 (1.50)	77.2 (1.32)	79.0 (1.03)	78.7 (2.37)	78.2 (1.44)	78.8 (1.59)
$\frac{Ca}{Si}$	1.83 (0.073)	1.57 (0.139)	1.84 (0.131)	1.79 (0.125)	1.91 (0.111)	1.82 (0.124)
$\frac{Al+Fe}{Ca}$	0.062 (0.0149)	0.092 (0.0178)	0.046 (0.0102)	0.087 (0.0174)	0.063 (0.0256)	0.099 (0.0279)
$\frac{S}{Ca}$	0.018 (0.0056)	0.050 (0.0077)	0.019 (0.0029)	0.040 (0.0060)	0.032 (0.0085)	0.046 (0.0063)

FIG. 8.
Backscattered electron image of 0.50 w/c ratio cement paste cured at constant temperature of 5°C to a degree of hydration of 70%.

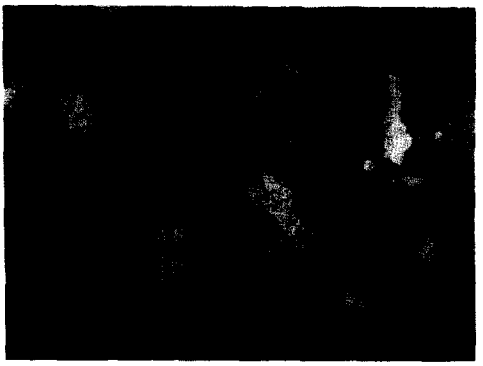

FIG. 9.
Backscattered electron image of the 0.50 w/c ratio cement paste cured at 50°C to a degree of hydration of 70%.

others due to the drying. The hollow shell porosity is generally higher at lower degrees of hydration (19). Possible reasons for the apparently higher hollow shell porosity of concrete B than of concrete A will be discussed in more detail later. It is observed that the hollow shell porosity of concretes A and B is generally higher in the zone close to the aggregates than in the bulk phase, in agreement with the results reported in (20) and (21). For concrete C the hollow shell porosity appears to be very high both in the interfacial zone and in the bulk paste. Table 1 shows the measured atomic ratios and the analyses of the inner and outer products of the concretes cured according to regime A, B or C. All pairs of means were compared by Duncan's

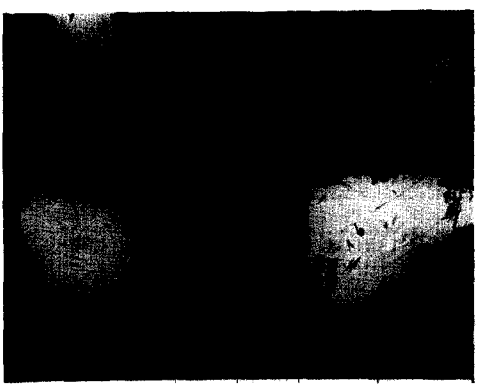

FIG. 10.
Backscattered electron image of the 0.50 w/c ratio cement paste cured at 50°C up to 30% hydration, followed by curing at 5°C to a degree of hydration of 70%.

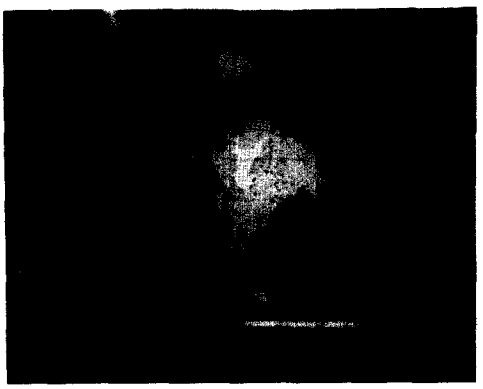

FIG. 11.
Detailed image of the cement paste shown in Fig.8.

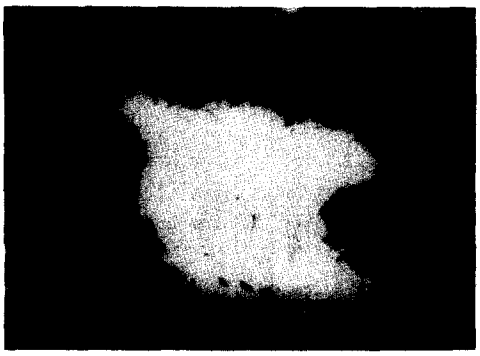

FIG. 12.
Detailed image of the cement paste shown in Fig.9.

Multiple Range Test (22) at a significance level of 5%. The statistical analysis revealed no significant difference as regards total oxides. The Ca/Si ratio of the outer product phase of concrete A was found to be significantly lower than the others. The Ca/Si ratio of the outer product of concrete B was significantly lower than that of the inner product of concrete C; otherwise there were no significant differences. The (Al+Fe)/Ca and S/Ca atomic ratios of the C-S-H phases appear to be higher in the outer product than in the inner product.

In addition to the concretes, some previously studied (8,9) cement paste specimens cured at various temperatures have been reanalyzed. These specimens were isothermally cured at 5°C or 50°C, one specimen (50°C/5°C) was cured at 50°C up to about 30% hydration (about 4 hours) and thereafter cured at 5°C. The specimens were sealed cured; thus there was no moisture exchange with the environment. Hydration was stopped when the cement had hydrated

TABLE 2

Atomic Ratios and Total Oxide of the Inner- and Outer- Product Phases of the 0.31 w/b Ratio Concrete Specimens Cured According to Cycles A, B and C
(Mean values; standard deviations in parantheses)

	5°C		50°C		50°C/5°C	
	Inner product	Outer product	Inner product	Outer product	Inner product	Outer product
Total oxide (%)	64.1 (5.50)	62.0 (4.14)	73.3 (1.85)	65.9 (3.16)	68.9 (1.77)	66.4 (3.16)
$\frac{Ca}{Si}$	1.99 (0.157)	2.05 (0.151)	2.10 (0.113)	1.95 (0.116)	1.95 (0.272)	2.01 (0.157)
$\frac{Al+Fe}{Ca}$	0.084 (0.0233)	0.065 (0.0129)	0.052 (0.0090)	0.091 (0.0397)	0.070 (0.0183)	0.077 (0.0218)
$\frac{S}{Ca}$	0.015 (0.0120)	0.059 (0.0151)	0.0299 (0.0090)	0.074 (0.0197)	0.0130 (0.0108)	0.060 (0.0102)

moisture exchange with the environment. Hydration was stopped when the cement had hydrated to about 70% and the flat polished specimens were examined by backscattered electron imaging. The result of a limited SEM-EDX analysis were reported previously (23). In the present work the composition of the inner and outer C-S-H product phases were studied by SEM-EDX. Figs.8 and 9 show the specimens cured at 5 and 50°C, respectively. The 50°C/5°C specimen is depicted in Fig.10. Figs.11 and 12 show more detailed images of the 5 and 50°C cured specimens. By comparing Figs.8, 9, 11 and 12 it appears that the reaction products are more evenly distributed throughout the matrix in the specimen hydrated at 5°C, while at 50°C the inner product appears considerably denser than the outer product, as previously reported (9). The measured elemental ratios and the sum of oxides are presented in Table 2. The statistical analysis showed no significant difference in the Ca/Si ratios. The total oxide content of the inner product of the specimen cured at 50°C was found to be significantly higher than that of the others, except for the inner product of the specimen first hydrated at 50°C and subsequently at 5°C. Otherwise there were no significant differences. As with the concretes, the S/Ca ratio appear to be higher in the outer product than in the inner product. There is possibly a trend of higher S/Ca ratio in both the inner and outer product of the 50°C specimen compared to the two others. Regarding the (Al+Fe)/Ca ratios, the 50°C specimen follows the same trend as the concretes with a higher (Al+Fe)/Ca ratio in the outer product than in the inner product. However, the opposite is observed in the 5°C specimen.

Discussion

The microanalysis only rarely revealed AFt phases while phases with compositions close to that of AFm were relatively frequently identified in all specimens. This microanalytical observation is in accordance with that made by Scrivener and Taylor (16). Based on additional X-ray diffraction analysis, they hypothesized that AFt most likely was present but was intimately mixed with the C-S-H gel and thus was not readily detectable by microanalysis since additional Al was assumed to be incorporated in the C-S-H gel. Curing at elevated temperatures has been reported to lead to less formation of AFt and AFm at the time of heat treatment (13-16,24). Aluminum, ferrite and sulfate ions will instead increasingly be present in the pore solution or adsorbed or substituted in the C-S-H structure. After heat treatment AFt and AFm will slowly reform. The analysis of the C-S-H phases in the present study showed average S/Ca ratios in the range 0.013 to 0.074 and average (Al+Fe)/Ca ratios in the range 0.046 to 0.099. This indicates intimate mixing with small amounts of AFt or AFm or possibly are Al, Fe and S ions present in the C-S-H gel in other ways, sorbed or substituted (16). The variations of the Ca/Si ratio from point to point within phases, seen from the standard deviation given in Tables 1 and 2, can be due to a variable C-S-H composition but also due to the presence of other hydrates at a small scale and possibly ionic substitution. For example, microcrystalline CH has been identified within the C-S-H structure (25).

The S/Ca and (Al+Fe)/Ca ratios were generally higher in the outer product than in the inner product in accordance with that often reported at room temperature (26,27). It is possible that the (Al+Fe)/Ca ratio of the inner product decreases with an increase in curing temperature from 20 to 65°C, in agreement with that reported for temperatures ranging from 25 to 80°C (28). Apparently the curing temperature influences the distribution of Al and Fe at low temperatures. The inner product of the cement paste specimen cured at 5°C appears to have a higher (Al+Fe)/Ca ratio than the outer product, in contrast to the specimen cured at 50°C, which shows

the same trend as the concretes. The relatively low (Al+Fe)/Ca ratio of the outer product and the relatively high ratio of the inner product of the specimen cured at 5°C indicates that less Al and Fe have migrated from the reaction sites of the anhydrous phases into the outer product. Probably, Al and Fe migrate much less readily at such low temperatures as 5°C. The fact that large AFm phases often form in previously formed hollow shells (23) of the specimens cured at 5°C supports this idea. Examples of AFm phases formed in previously formed hollow shells are shown in Figs.8 and 11 by arrows. Relatively high concentrations of Al and Fe in the pore solution within the hollow shells, which could result from a low diffusion rate of these species at low temperatures, will presumably promote the formation of AFm phases in previously formed hollow shells when sulfate ions diffuse into the shells. This can be one reason why distinct AFm formations up to 10 microns across frequently were observed in the 5°C and the 50°C/5°C specimens but not in the 50°C specimen. AFm phases were detected by microanalysis in the 50°C specimen but then as much smaller formations presumably in the capillary pores or intermixed with C-S-H.

It appears from Figs.8, 9, 11 and 12 that the C-S-H inner product of the pastes cured isothermally at 50°C are much denser than the corresponding phase in pastes cured at 5°C. Gray level histograms of backscattered electron images of the same specimens confirm this impression (29). It has been hypothesized (11) that the brighter hydration shells formed around the cement grains at higher curing temperatures could be due to closer mixing of CH with the C-S-H, and increasing Ca/Si ratios of the "in situ" gel have been reported (16,28). Due to the higher atomic number of Ca as compared to Si, the presence of closely mixed CH or a higher Ca/Si ratio of the C-S-H phases, will result in a gray level of increased brightness. However, the microanalysis given in Table 2 revealed no significant difference between any of the Ca/Si ratios. This result is in agreement with preliminary findings (23,30). On the other hand, the statistics showed the analysis total of the inner product of the specimen cured at 50°C to be significantly higher than those of most of the others. The analysis total should primarily depend on the concentration of the energy dispersive X-ray detectable elements and their oxides present in the sampling volume, although its significance may be more complicated (31).

Water is removed during the preparation of the specimen except most of that structurally incorporated in the gel. The larger pores are refilled with epoxy resin, while the smallest pores including the interlayer space presumably will remain largely empty after specimen preparation. Some water and solids may also evaporate during analysis. The difference in analysis total from 100% is assumed to approximate the amount of water present in any state in addition to the amount of polymer- or air-filled pores or interlayer spaces present in the microvolume subjected to analysis. Although reaction products poorer in chemically bound water have been reported to form at elevated temperatures (32), no indications were found that the reaction products formed at 50°C contained less overall non-evaporable water than the reaction products formed at 20 or 5°C (9). Assuming constant water chemically bound in the C-S-H gel, the greater total oxides in the inner product of the sample cured at 50°C suggest that this phase has a somewhat lower fine porosity than the outer product or hydrated phases of the specimen cured at 5°C.

Fine porosity could be expected to incorporate interlayer space and/or micro- and mesopores. Minimal low fine porosity of the inner product of the specimen cured at 50°C would explain its higher gray level brightness. Figs.11 and 12 show that the outer product of the specimen cured at 50°C contains a higher fraction of large capillary pores than the outer product of the specimen cured at 5°C. The increased porosity of the outer product of the specimen cured at 50°C was reported to be about 0.25 to 1.25 microns (8). (The lower size limit is inferred with some uncertainty because of limitations regarding resolution). The oxide totals given in Table

2 indicate that the local finer porosity of the outer C-S-H gel is largely independent of curing temperature. The present observations and reanalysis confirm earlier conclusions (8,9) that the reaction products are relatively evenly distributed throughout the cement paste matrix at low curing temperatures. At higher curing temperatures the C-S-H in the inner product apparently becomes denser primarely due to lower fine porosity and the outer product contains relatively coarse pores. The specimen cured initially at 50°C and later at 5°C has a microstructure and composition somewhat in between those resulting from the 5 and 50°C isothermal curing regimes, although more like those of the specimen cured at 5°C. Thus it appears that the temperature at somewhat greater maturities is more important than that at early ages as regards the final distribution of C-S-H. This was noted earlier (9) and possible explanations have been deduced (33).

Microanalytical and microscopical examination of the 0.31 w/b ratio concrete supports the idea that the early curing temperature has relatively little influence on the final distribution of C-S-H. The inner product of heat cured concrete does not appear denser than that of concrete cured at 20°C, and the outer product does not appear to have a higher porosity. The 0.50 w/c ratio cement paste non-isothermally cured had reached considerably less maturity at the end of its heat curing period and showed, in contrast to the heat cured concrete, some influence of the heat curing as regards C-S-H distribution. The difference can at least partly be ascribed to the different reference temperatures and the difference in temperature during the post-heat curing period (20°C vs 5°C). The different moisture conditions, w/b ratios and binder and mix compositions may also be influential factors. At medium to high w/b ratios, heat treatment is generally reported to result in a coarsening of the pore structure, greater capillary pore volumes, and increased MIP "threshold" diameters (4-7). Different results have been found at low w/b ratios. Odler et al. (34) reported that the pore structure was largely uninfluenced by the curing temperature at a w/b ratio of 0.2. Justnes and Havdahl (35) reported that the MIP porosity decreased with increasing initial temperature of cement pastes of w/b ratio 0.25 with silica fume. This suggests that the resulting effect of heat curing on the distribution of C-S-H depends on the mix composition. It appears that at very low w/b ratios, where silica fume are customarily added, the influence of elevated curing temperatures on the C-S-H distribution, as seen at high w/c ratios, diminishes. The outer product may become less permeable by lower porosity or finer porosity.

The largest gray level contrast between inner and outer product of the concretes is seen in that cured at 20°C. The Ca/Si ratio of the outer product was found to be significantly lower than that of the other phases. It appears from the backscattered electron images along with additional X-ray point analysis of the concrete cured at 20°C that CH formed in many previously formed hollow shells of this specimen. This is presumably one reason for the apparently lower hollow shell porosity and this can also be one reason for the low Ca/Si ratio of the outer product. Calcium ions may have diffused into the previously formed hollow shells and precipitated as CH. This phenomenon was not seen to the same extent in the heat cured concrete also subsequently water cured, possibly due to the greater maturity of the heat cured concrete at the time of exposure to water curing. As discussed previously, the concrete stored outdoors after heat curing has a higher hollow shell porosity and capillary porosity. The removal of water from the pore system due to drying has presumably reduced the hydration rate considerably. The hollow shell porosity is higher partly due to the lower degree of hydration and partly because less hydration products can be deposited in hollow shells which probably have been largely dried out. The fine porosity appears not to have been significantly influenced by drying.

Conclusions

At later ages, the inner product phase of 0.50 w/c ratio cement paste isothermally cured at 50°C revealed a lower fine porosity than that of its outer product phase or the inner product phase of a companion specimen cured at 5°C. The Ca/Si ratios of the inner and outer product were apparently not influenced by curing temperature. The distribution of reaction products (C-S-H) throughout the cement paste matrix at later ages was much more uniform at relatively low curing temperatures.

Heat cured 0.31 w/b ratio concrete showed a higher hollow shell porosity at later ages than its companion cured at 20°C. Less CH formed in previously formed hollow shells in the heat cured concrete, which is at least one reason for its higher hollow shell porosity. High performance concrete heat cured and then stored outdoors showed the highest hollow shell porosity and capillary porosity as revealed from backscattered electron images. The distribution of C-S-H in the bulk paste matrix was apparently not much influenced by heat curing. On the other hand, the composition of the C-S-H phases was influenced by the curing regime.

It appears that the (Al+Fe)/Ca ratio of the inner product phase increases with decreasing curing temperature. Probably, Al and Fe diffuse less readily at low temperatures. This may influence the distribution and formation of the AFt and AFm phases in the matrix. In plain cement pastes cured at 50°C, AFm apperently formed as small crystals in the capillary pores or intermixed with C-S-H at later ages. In pastes cured at 5°C, AFm formed large phases (up to over 10 microns across) in previously formed hollow shells at later ages.

Acknowledgement

I would like to thank Dr. R.J. Detwiler and Dr. H. Justnes for valuable discussions.

References

1. F.A Oluokun, E.G. Burdette and J.II. Deatherage, Transp.Res.Rec., No.1284, National Research Council, Washington D.C., 31 (1990).
2. J-E. Jonasson, Proc.3rd Int. RILEM Symp.on Winter Concreting, Espoo, 249 (1985)
3. R.J. Detwiler, C.A. Fapohunda and J. Natale, ACI Mater.J. 91, 63 (1994).
4. J. Skalny and I. Odler, J.Colloid Interface Sci. 40, 199 (1972).
5. A. Bentur, R.L. Berger, J.H. Kung, N.B. Milestone and J.F. Young, J.Am.Ceram.Soc. 62, 362 (1979).
6. E.J. Sellevold, Cem.Concr.Res. 4, 399 (1974).
7. S. Goto and D.M Roy, Cem.Concr.Res. 11, 575 (1981).
8. K.O. Kjellsen, R.J. Detwiler and O.E. Gjørv, Cem.Concr.Res. 20, 927 (1990).
9. K.O. Kjellsen, R.J. Detwiler and O.E. Gjørv, Cem.Concr.Res. 21, 179 (1991).
10. J.H. Taplin, Austr.J.Appl.Sci. 10, 329 (1959).
11. H.F.W. Taylor, Adv.Cem.B.Mater. 1, 38 (1993).
12. G.J. Verbeck and R.H. Helmuth, Proc.5th ICCC, Tokyo 3, 1 (1968).
13. H.Y. Ghorab, D. Heinz, U. Ludwig, T. Meskendahl and A. Wolter, Proc.7th ICCC, Paris 4, 496 (1980).
14. D. Heinz and U. Ludwig, Proc.8th ICCC, Rio de Janeiro 5, 189 (1986).
15. H.M. Sylla, Beton 38, 449 (1988).
16. K.L. Scrivener and H.F.W.Taylor, Adv.Cem.Res. 5, 139 (1993).
17. J. Alexanderson, Proc.No.43, Swedish Cem.Concr.Res.Inst. Stockholm, 135pp (1972).

18. S. Diamond and D. Bonen, J.Am.Ceram.Soc. 76, 2993 (1993).
19. K.O. Kjellsen, H.M. Jennings and B. Lagerblad, submitted for publication.
20. D.W. Hadley, PhD Thesis, Purdue University, USA, 186pp (1972).
21. K.L. Scrivener and E.M. Gartner, MRS Symp.Proc., Mater.Res.Soc. 114, 77 (1988).
22. D.C. Montgomery, Design and Analysis of Experiments, John Wiley & Sons, 2nd Ed., New York, 538 pp. (1984).
23. K.O. Kjellsen and R.J. Detwiler, Proc.9th ICCC, New Delhi 4, 241 (1992).
24. W. Wieker, T. Bade, A. Winkler and R. Herr, Proc. RILEM Workshop Hydration and Setting of Cements, E & FN Spon, London, 125 (1992).
25. G.W. Groves, Cem.Concr.Res. 11, 713, (1981).
26. I.G. Richardson and G.W. Groves, J.Mater. Sci. 28, 265 (1993).
27. D. Bonen and S. Diamond, J.Am.Ceram.Soc. 77, 1875 (1994).
28. A.K. Crumbie, P.L. Pratt and H.F.W. Taylor, Proc.9th ICCC, New Delhi 4, 131 (1992).
29. K.O. Kjellsen, R.J. Detwiler and O.E. Gjørv, Cem.Concr.Res. 20, 308 (1990).
30. K.L. Scrivener, Cem.Concr.Res. 22, 1224 (1992).
31. A.M. Harrison, N.B. Winter and H.F.W. Taylor, J.Mater.Sci.Lett. 6, 1339 (1987).
32. I. Odler and J. Skalny, J.Appl.Chem.Biotechnol. 23, 661 (1973).
33. K.O. Kjellsen and R.J. Detwiler, Cem.Concr.Res. 22, 112 (1992).
34. I. Odler, J. Hagymassy, E.E. Bodor, M. Yudenfreund and S. Brunauer, Cem.Concr.Res. 2, 577 (1972).
35. H. Justnes and J. Havdahl, Proc.Int.Conf. Blended Cements in Construction, Elsevier Applied Science, London, 138 (1991).